

# On the Shapes of Interstellar Grains: Modeling Infrared Extinction and Polarization by Spheroids and Continuous Distributions of Ellipsoids

B. T. Draine and Brandon S. Hensley to

Department of Astrophysical Sciences, Princeton University, Princeton, NJ 08544-1001, USA; draine@astro.princeton.edu, bhensley@astro.princeton.edu

Received 2020 November 12; revised 2021 January 17; accepted 2021 January 18; published 2021 March 25

#### Abstract

Although interstellar grains are known to be aspherical, their actual shapes remain poorly constrained. We assess whether three continuous distributions of ellipsoids (CDEs) from the literature are suitable for describing the shapes of interstellar grains. Randomly selected shapes from each distribution are shown as illustrations. The oftenused Bohren–Huffman CDE includes a very large fraction of extreme shapes: fully 10% of random draws have axial ratio  $a_3/a_1 > 19.7$ , and 5% have  $a_3/a_1 > 33$ . The CDE2 distribution includes a much smaller fraction of extreme shapes, and appears to be the most realistic. For each of the three CDEs considered, we derive shape-averaged cross sections for extinction and polarization in the Rayleigh limit. Finally, we describe a method for "synthesizing" a dielectric function for an assumed shape or shape distribution if the actual absorption cross sections per grain volume in the Rayleigh limit are known from observations. This synthetic dielectric function predicts the wavelength dependence of polarization, which can then be compared to observations to constrain the grain shape.

Unified Astronomy Thesaurus concepts: Interstellar dust (836)

#### 1. Introduction

After many years of study, both the composition and the geometry (shape, porosity) of interstellar grains remain uncertain. While meteorites can provide samples of presolar grains that were part of the interstellar grain population at the time of formation of the solar system, the surviving particles may not be representative, and the sampling techniques are biased toward large "stardust" grains with isotopic anomalies. Interstellar grains collide with interplanetary spacecraft, providing some information on elemental composition, but the data are limited and generally involve vaporization of the impinging particle, leaving both mineralogy and preimpact morphology uncertain (e.g., Altobelli et al. 2016). The Stardust mission captured some particles relatively intact (Westphal et al. 2014a, 2014b), but dynamical considerations argue against these particles having come from the interstellar medium (Silsbee & Draine 2016).

As a result, our knowledge of interstellar grains is based almost entirely on (1) evidence of elements that have been "depleted" from interstellar gas and incorporated into dust grains and (2) observations of the interaction of electromagnetic waves with the interstellar grains: absorption, scattering, and emission (Hensley & Draine 2021). The challenge to grain modelers is to create physical models that are consistent with these constraints.

Grain models must specify the optical properties of the grain materials, and the shapes and sizes of the grains. The optical properties of a grain, particularly for polarization, depend on the grain shape, i.e., morphology. Because the universe of possible grain morphologies is unbounded, modelers are forced to limit consideration to some subset of idealized shapes. With stringent constraints now available for polarized extinction by and emission from interstellar grains, the assumption of spherical grains is no longer adequate for modeling. The natural first step beyond spheres is to consider spheroids and ellipsoids.

The present work has two aims. The first is to discuss certain distributions of ellipsoidal shapes. Continuous distributions of

spheroidal or ellipsoidal shapes have been considered in some previous studies, but the discussions have generally been limited to the angle-averaged absorption cross sections, with little said about the actual distribution of *shapes*. Here we explicitly discuss the distribution of shapes associated with three particular continuous distributions of ellipsoids (CDEs). We also derive the polarization cross sections for the CDEs for grains in the "electric dipole" or Rayleigh limit when the grains are not randomly oriented.

The second aim is to present a method for using observational constraints on absorption at long wavelengths, plus a prior estimate of the dielectric function at shorter wavelengths, to derive the complex dielectric function  $\epsilon(\lambda)$  at long wavelengths  $\lambda$ . Absorption and polarization by grains both depend on the grain shape, or distribution of shapes. If we knew the dielectric function  $\epsilon(\lambda)$ , we could (at least in principle) infer the actual grain shape by computing absorption versus  $\lambda$  for different assumed shape distributions, and seeing which shape distribution best agrees with observations. Because the actual grain materials remain unknown, we do not know  $\epsilon(\lambda)$ , and hence cannot use that approach to deduce the grain shape. However, if we have observations of both absorption and polarization, we can determine which shape distribution yields a dielectric function that is consistent with both. We show here how this can be done. The methods developed here have been employed to obtain a dielectric function for "astrodust" (Draine & Hensley 2021) for spheroids and CDEs.

The paper is organized as follows: absorption and polarization cross sections for ellipsoids in the long-wavelength (Rayleigh) limit are reviewed in Section 2. In Section 3, we discuss the properties of three continuous distributions of ellipsoidal shapes, the BHCDE, ERCDE, and CDE2 distributions, and present images of shapes drawn randomly from each of these distributions. Analytic results for polarized absorption cross sections are presented in Sections 4 and 5. Attenuation and polarization by a medium with partial grain alignment is discussed in Section 6. In Section 7, we develop a method for employing the results obtained here, together with other

<sup>1</sup> Spitzer Fellow.

constraints, to obtain a self-consistent dielectric function given observations of absorption as a function of wavelength. Our results are summarized in Section 9. Certain technical results are collected in Appendices A–D.

#### 2. Absorption in the Rayleigh Limit

In the Rayleigh limit (grain size  $\ll$  wavelength  $\lambda$ ), the interaction of a grain with an incident electromagnetic wave is fully characterized by the grain's electric polarizability tensor (see, e.g., Draine & Lee 1984). Here we review the dependence of this polarizability tensor on the grain shape.

## 2.1. Ellipsoidal Grains

Consider an ellipsoidal grain with semimajor axes  $a_1 \leq a_2 \leq a_3$  and volume  $V = (4\pi/3)a_1a_2a_3$ . Let  $\hat{a}_1$ ,  $\hat{a}_2$ ,  $\hat{a}_3$  be unit vectors along the three principal axes. We define an effective radius  $a_{\rm eff} \equiv (3V/4\pi)^{1/3} = (a_1a_2a_3)^{1/3}$ .

The grain material is assumed to have an isotropic complex dielectric function  $\epsilon(\lambda) = \epsilon_1 + i\epsilon_2$ , where  $\epsilon_1(\lambda)$  and  $\epsilon_2(\lambda)$  are the real and imaginary parts of  $\epsilon$ , and  $\lambda$  is the wavelength *in vacuo*. In the long-wavelength limit  $a_3 \ll \lambda$ , the electric polarizability tensor for radiation with  $E\|\hat{a}_j$  is  $\alpha_{ij} = A_j V/4\pi$ , where

$$A_j(\epsilon) = \frac{\epsilon - 1}{1 + L_j(\epsilon - 1)}, \qquad (1)$$

with  $L_i$  given by (see, e.g., Bohren & Huffman 1983)

$$L_{j} = \frac{1}{2} \int_{0}^{\infty} \frac{dx}{[y_{j}^{2} + x][(y_{1}^{2} + x)(y_{2}^{2} + x)(y_{3}^{2} + x)]^{1/2}}$$
 (2)

$$y_j \equiv \frac{a_j}{(a_1 a_2 a_3)^{1/3}}. (3)$$

The  $L_j$ , referred to variously as "geometrical factors," "shape factors," or "depolarization factors" are determined by the axial ratios  $a_1/a_3$  and  $a_2/a_3$ . The  $L_j$  satisfy

$$L_1 + L_2 + L_3 = 1. (4)$$

If  $a_1 \leqslant a_2 \leqslant a_3$ , then

$$L_1 \geqslant L_2 \geqslant L_3. \tag{5}$$

The allowed domain is shown in Figure 1. The absorption cross section for radiation with  $E||\hat{a}_i|$  is

$$C_{\text{abs},j} = \frac{2\pi V}{\lambda} \operatorname{Im}(A_j). \tag{6}$$

After propagating a distance z through a medium with dust number density  $n_d$ , a plane wave will undergo both attenuation (due to absorption) and a phase shift relative to propagation *in vacuo*. The phase shift (in radians) will be  $n_d C_{\text{pha}} z$ , where

$$C_{\text{pha},j} = \frac{\pi V}{\lambda} \operatorname{Re}(A_j).$$
 (7)

The axes  $\hat{a}_1$ ,  $\hat{a}_2$ ,  $\hat{a}_3$  coincide with the principal axes of the moment of inertia tensor, with eigenvalues  $I_1 \ge I_2 \ge I_3$ . For randomly oriented grains, the absorption cross section is

$$C_{\text{ran}} = \frac{C_{\parallel} + 2C_{\perp}}{3} = \frac{2\pi V}{\lambda} \text{Im} \left( \frac{A_1 + A_2 + A_3}{3} \right).$$
 (8)

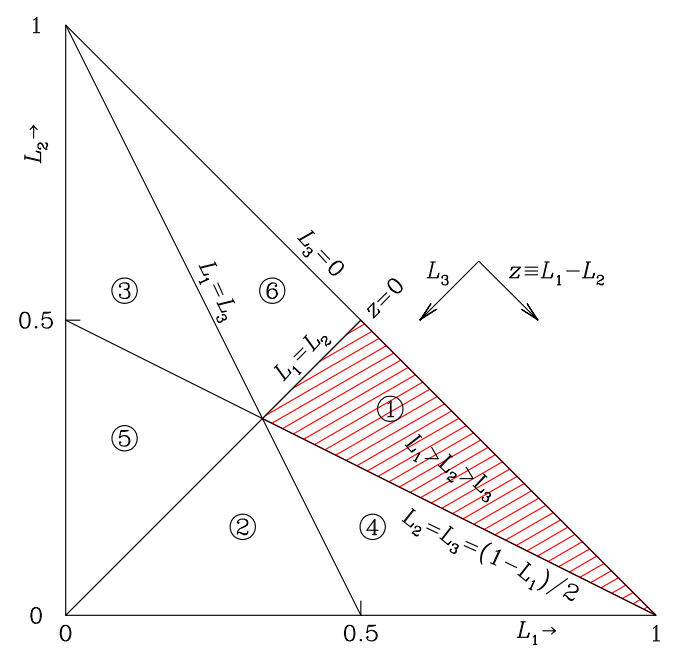


**Figure 1.** The domain of allowed shape factors  $(L_1, L_2)$ . The shaded region is the domain where  $L_3 \le L_2 \le L_1$  (see text). Other regions, numbered 2–6, correspond to the other possible orderings of  $L_1$ ,  $L_2$ ,  $L_3$ .

Interstellar grains are generally spinning rapidly, and it is appropriate to average over the grain orientations. The direction of the grain axis  $\hat{a}_1$  may be correlated with the angular momentum vector J; if the grains are in suprathermal rotation,  $\hat{a}_1$  will tend to be aligned with J, as originally pointed out by Purcell (1979). The absorption cross sections for  $E||\hat{a}_1|$  and  $E\perp\hat{a}_1$  are

$$C_{\parallel} \equiv C_{\text{abs}}(E||\hat{\boldsymbol{a}}_{1}) = \frac{2\pi V}{\lambda} \operatorname{Im}(A_{1})$$
 (9)

$$C_{\perp} \equiv C_{\text{abs}}(E \perp \hat{\boldsymbol{a}}_1) = \frac{2\pi V}{\lambda} \operatorname{Im}\left(\frac{A_2 + A_3}{2}\right),$$
 (10)

where the grains are assumed to be spinning with  $\hat{a}_2$  and  $\hat{a}_3$  randomly distributed in the plane  $\perp$  to  $\hat{a}_1$ .

Consider the limiting case of spinning grains that are perfectly aligned with  $\hat{a}_1 || J$ . For unpolarized radiation propagating with wave vector  $k \perp J$ , the polarization-averaged absorption cross section is

$$C_{\text{abs}} = \frac{C_{\perp} + C_{\parallel}}{2} = \frac{2\pi V}{\lambda} \operatorname{Im} \left( \frac{A_2 + A_3 + 2A_1}{4} \right).$$
 (11)

The difference in absorption cross sections will produce linear polarization, characterized by the "polarization cross section"

$$C_{\text{pol}} = \frac{C_{\perp} - C_{\parallel}}{2} = \frac{2\pi V}{\lambda} \operatorname{Im} \left( \frac{A_2 + A_3 - 2A_1}{4} \right).$$
 (12)

There will also be a phase shift between the two linear polarizations. We define

$$\Delta C_{\text{pha}} \equiv C_{\text{pha},\perp} - C_{\text{pha},\parallel} = \frac{\pi V}{\lambda} \operatorname{Re} \left( \frac{A_2 + A_3 - 2A_1}{2} \right). \quad (13)$$

After propagating a distance z through a medium with dust number density  $n_d$ , the phase difference between the modes will

be  $n_d \Delta C_{\text{pha}} z$ . If the direction of grain alignment rotates along the direction of propagation, radiation that is initially unpolarized will develop circular polarization (Martin 1972, 1974). We define a "circular polarization efficiency factor"

$$Q_{\rm cpol} \equiv \frac{C_{\rm pol}}{\pi a_{\rm eff}^2} \times \frac{\Delta C_{\rm pha}}{\pi a_{\rm eff}^2}.$$
 (14)

If the rotation angle is small, and the percentage linear polarization is small, the circular polarization after propagating a path length z has Stokes parameters V and I varying as

$$\frac{V}{I} \propto Q_{\rm cpol} \times (n_d \pi a_{\rm eff}^2 z)^2. \tag{15}$$

# 2.2. Spheroids

Prolate spheroids have  $a_1 = a_2 < a_3$ , and oblate spheroids have  $a_1 < a_2 = a_3$ . The "shape factors"  $L_i$  are given by van de Hulst (1957)

prolate: 
$$L_3 = \frac{1 - e^2}{e^2} \left[ \frac{1}{2e} \ln \left( \frac{1 + e}{1 - e} \right) - 1 \right] < 1/3, \ e^2 \equiv 1 - \left( \frac{a_1}{a_3} \right)^2$$
(16)

$$L_1 = L_2 = \frac{1 - L_3}{2} \tag{17}$$

oblate: 
$$L_1 = \frac{1+e^2}{e^2} \left[ 1 - \frac{1}{e} \arctan(e) \right] > 1/3, \ e^2 \equiv \left( \frac{a_3}{a_1} \right)^2 - 1$$
 (18)

$$L_2 = L_3 = \frac{1 - L_1}{2}. (19)$$

A sphere has  $(L_1, L_2, L_3) = (\frac{1}{3}, \frac{1}{3}, \frac{1}{3})$ ; the prolate limit (needlelike) has  $(L_1, L_2, L_3) = (\frac{1}{2}, \frac{1}{2}, 0)$ ; the oblate limit (disk-like) has  $(L_1, L_2, L_3) = (1, 0, 0)$ .

#### 3. Continuous Distributions of Ellipsoids

#### 3.1. Shape Factors

Every ellipsoidal shape is uniquely specified by its triplet of depolarization factors  $(L_1, L_2, L_3)$ . Consider a population of ellipsoidal grains, each with the same volume V, but with some continuous distribution of axial ratios; this is referred to as a "continuous distribution of ellipsoids" (CDE). Suppose that each grain has principal axes labeled 1,2,3 arbitrarily, and that  $G(\ell_1,$  $\ell_2$ ) $d\ell_1d\ell_2$  is the fraction of the population with  $L_1 \in [\ell_1, \ell_1 + d\ell_1]$ ,  $L_2 \in [\ell_2, \ \ell_2 + d\ell_2]$ , and  $L_3 = 1 - L_1 - L_2$ . The function G is nonnegative  $(G \geqslant 0)$  and normalized:  $\int G(L_1, L_2) dL_1 dL_2 = 1$  over the allowed  $(L_1, L_2)$  domain. If labels 1,2,3 were assigned arbitrarily, the function G must satisfy symmetry requirements, including  $G(L_1, L_2) = G(L_2, L_1) = G(L_1, 1 - L_1 - L_2)^2$  but otherwise we have no a priori knowledge of the function G, other than expecting that very extreme axial ratios should be

Various distributions of shapes have been considered in the literature, including spheroids (Treffers & Cohen 1974; Min et al. 2003), and ellipsoids (Bohren & Huffman 1983). Bohren & Huffman (1983) gave a lucid introduction to CDEs in general, and presented a simple illustrative example, referred to here as the BHCDE. We discuss the BHCDE and two other distributions of ellipsoids that have been considered in the astrophysical literature.

1. BHCDE: The simplest functional form

$$G(L_1, L_2) = 2 \text{ for } L_1 \geqslant 0, \ L_2 \geqslant 0, \ L_1 + L_2 \leqslant 1$$
 (20)

is often considered; Bohren & Huffman (1983) present this as an example, and it has subsequently been applied by a number of authors (e.g., Rouleau & Martin 1991; Alexander et al. 1994; Min et al. 2003, 2006, 2008; Sargent et al. 2006; Rho et al. 2018. Because  $G(L_1, L_2)$  is independent of  $L_1$  and  $L_2$ , it is sometimes asserted that "all shapes are equally probable" (Bohren & Huffman 1983) or "all shapes are equally weighted" (Sargent et al. 2006), seemingly suggesting that this is a "fair" sampling of ellipsoidal shapes. While it is correct that all ellipsoidal shapes are present, it is not clear how "all shapes are equally probable" is to be understood, given that shapes are not discrete and there is no commonly accepted metric for "shape space."

Although having the virtue of analytic simplicity, we will see below that the BHCDE distribution has an extreme representation of very elongated shapes, with  $L \rightarrow 0$ . We will argue that the BHCDE distribution seems unlikely to approximate grain shape distributions in nature, whether for desert sand or interstellar dust.

2. ERCDE: Zubko et al. (1996) proposed eliminating the most extreme shapes by truncating the distribution (20):

$$G(L_1, L_2) = \frac{2}{(1 - 3L_{\min})^2} \text{ for } L_1 \geqslant L_{\min},$$
  

$$L_2 \geqslant L_{\min}, L_1 + L_2 \leqslant 1 - L_{\min},$$
(21)

referring to this as the "externally restricted CDE" (ERCDE).  $L_{\min}$  is a free parameter. While removing extreme shapes with  $L_j \rightarrow 0$  or  $L_j \rightarrow 1$  is desirable, the ERCDE distribution still seems unphysical, as we will see below. Note that if  $L_{\min} \rightarrow 0$ , the ERCDE  $\rightarrow$  BHCDE. 3. *CDE2*: Ossenkopf et al. (1992) proposed the distribution

$$G(L_1, L_2) = 120L_1L_2L_3 = 120L_1L_2(1 - L_1 - L_2)$$
  
for  $L_1 \ge 0$ ,  $L_2 \ge 0$ ,  $L_1 + L_2 \le 1$ , (22)

which has the desirable behavior  $G \rightarrow 0$  for  $L_3 \rightarrow 0$  and  $L_1 \rightarrow 1$ . This distribution has subsequently been referred to as "CDE2" (Fabian et al. 2001; Sargent et al. 2006), and we shall so refer to it here.

The distribution functions  $G(L_1, L_2)$  for these three CDEs are shown in Figure 2.

#### 3.2. Shape Distributions

Because the optical properties of ellipsoids in the limit  $a \ll \lambda$ are determined by  $L_1$ ,  $L_2$ , and  $L_3 = 1 - L_1 - L_2$ , most discussions of CDEs have been concerned only with the distribution of  $L_i$  values, rather than the distributions of the ellipsoid axial ratios. However, it is of interest to examine the distributions of actual grain shapes that correspond to the BHCDE, ERCDE, and CDE2 distributions.

One can also consider functions G that do not satisfy these symmetry requirements, but in this case, one must restrict discussion to only one of the six subregions in Figure 1.

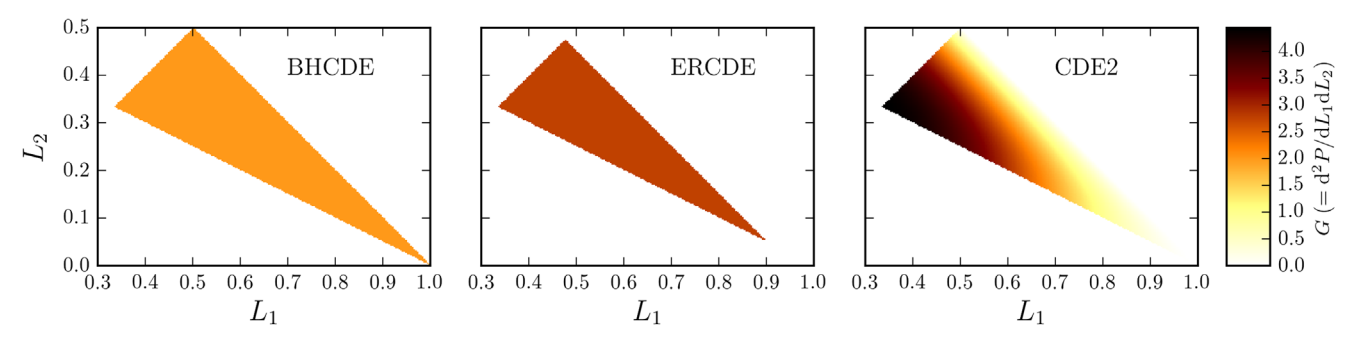
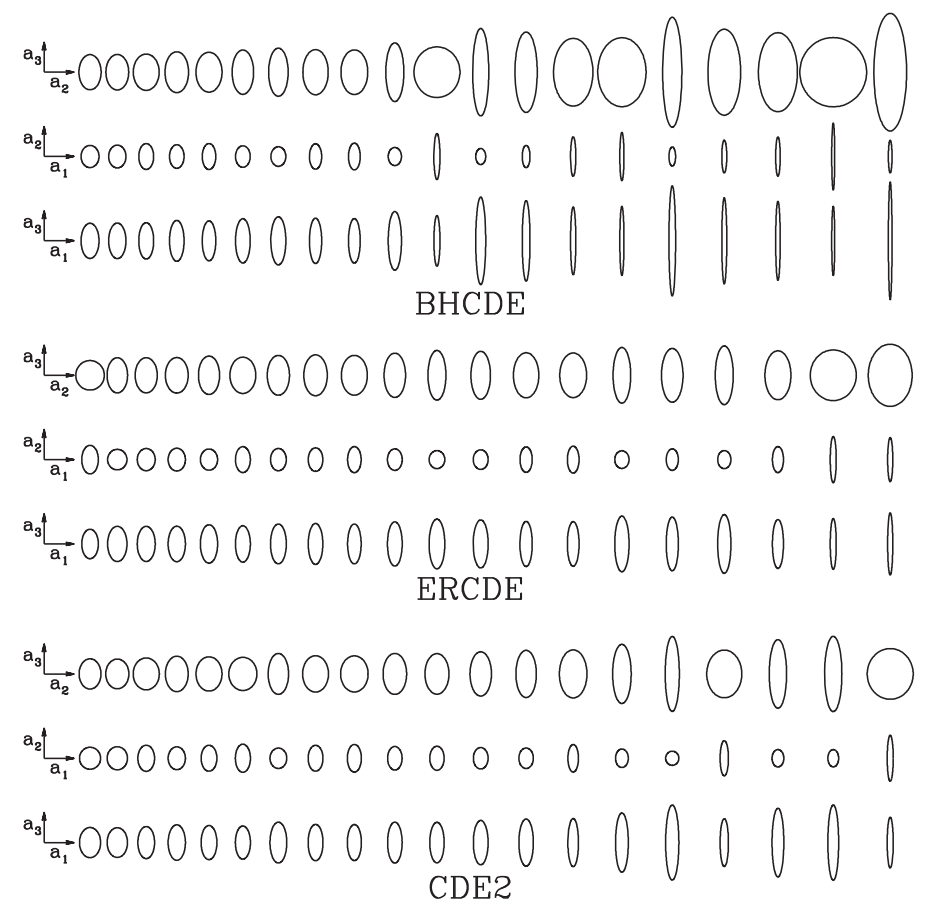


Figure 2.  $G(L_1, L_2)$  for the BHCDE, ERCDE (with  $L_{\min} = 0.05$ ), and CDE2 shape distributions.



**Figure 3.** Twenty randomly selected ellipsoids drawn from the BHCDE, ERCDE, and CDE2 distributions. All examples have equal volume. Three views are shown for each shape: viewed along the short axis  $\hat{a}_1$  (top row), and along the  $\hat{a}_3$  and  $\hat{a}_2$  axes (second and third rows). For each distribution, the 20 random shapes are shown in order of increasing  $a_3/a_1$  (left to right).

For a given set of axial ratios  $(a_2/a_1, a_3/a_1)$ , the  $L_j$  values can be obtained by numerical quadrature (Equation (2)). Since there does not appear to be any direct way to invert Equation (2) to obtain  $(a_2/a_1, a_3/a_1)$  from given  $(L_1, L_2)$ , we have implemented a numerical procedure to find  $(a_2/a_1, a_3/a_1)$  corresponding to given  $(L_1, L_2)$ . In Appendix D, we demonstrate that any solution found in this way is unique.

We continue to adopt the ordering  $a_1 \leqslant a_2 \leqslant a_3$ ,  $L_1 \geqslant L_2 \geqslant L_3$ . We draw  $(L_1, L_2)$  values randomly according to the BHCDE, ERCDE, or CDE2 distributions and, for each  $(L_1, L_2)$ , find the corresponding axial ratios  $(a_2/a_1, a_3/a_1)$ . Figure 3 shows 20 examples selected randomly from each of these shape

distributions. Figure 4(a) shows the distribution of long/short axial ratios  $a_3/a_1$  for the BHCDE, ERCDE (with  $L_{\rm min}=0.05$ ), and CDE2 distributions. Figure 4(b) shows the cumulative distribution function of axial ratios  $a_3/a_1$ , and Figure 5 shows the distributions of axial ratios for the BHCDE, ERCDE, and CDE2 distributions. Some characteristics of these shape distributions are listed in Table 1.

The BHCDE distribution has a very large fraction of extreme axial ratios; Figure 4(b) shows that 10% of the realizations have  $a_3/a_1 > 19.7$  and 1% of the realizations have  $a_3/a_1 > 98.5$ . Extreme elongation will increase the susceptibility to fragmentation in high-speed grain-grain collisions. Highly elongated grains may also be more vulnerable to centrifugal disruption if

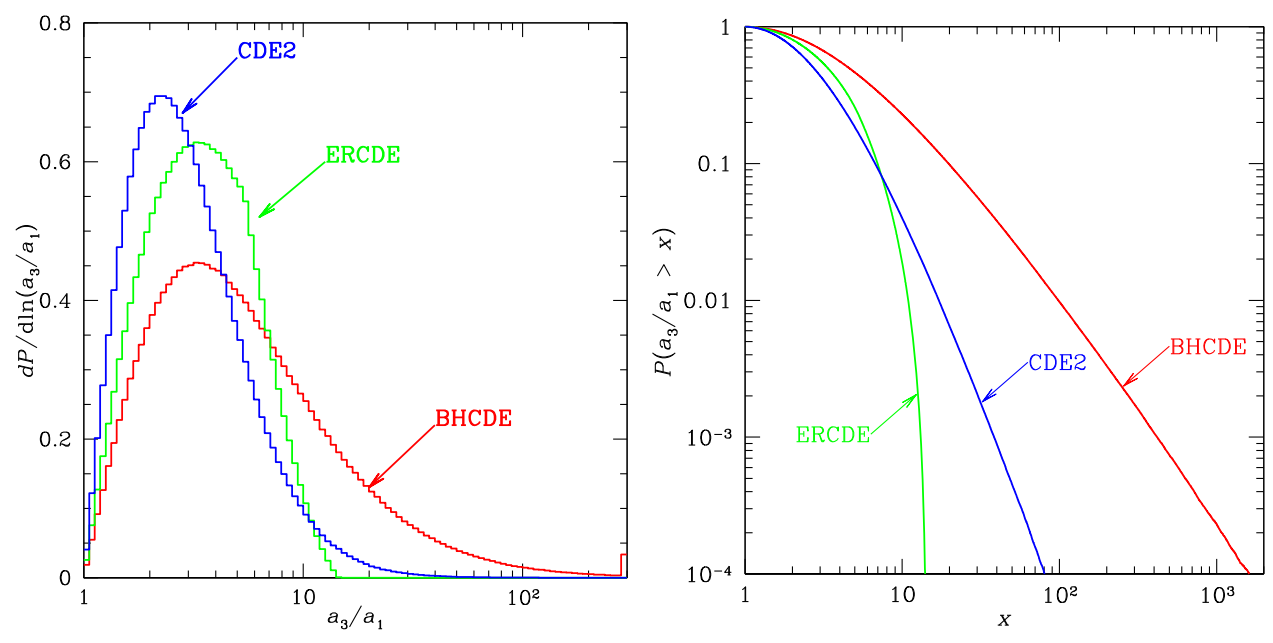


**Figure 4.** (a) Distribution of long/short axial ratio  $a_3/a_1$  for three continuous distributions of ellipsoids. The ERCDE with  $L_{\min} = 0.05$  has a maximum allowed axial ratio  $a_3/a_1 = 14$ , but the CDE2 and BHCDE distributions both extend to infinite axial ratios. The BHCDE distribution has a much larger representation of extreme axial ratios. (b) Cumulative distribution functions. For the BHCDE distribution, 10% of the realizations have  $a_3/a_1 > 19.7$ , and 1% have  $a_3/a_1 > 98.5$ .

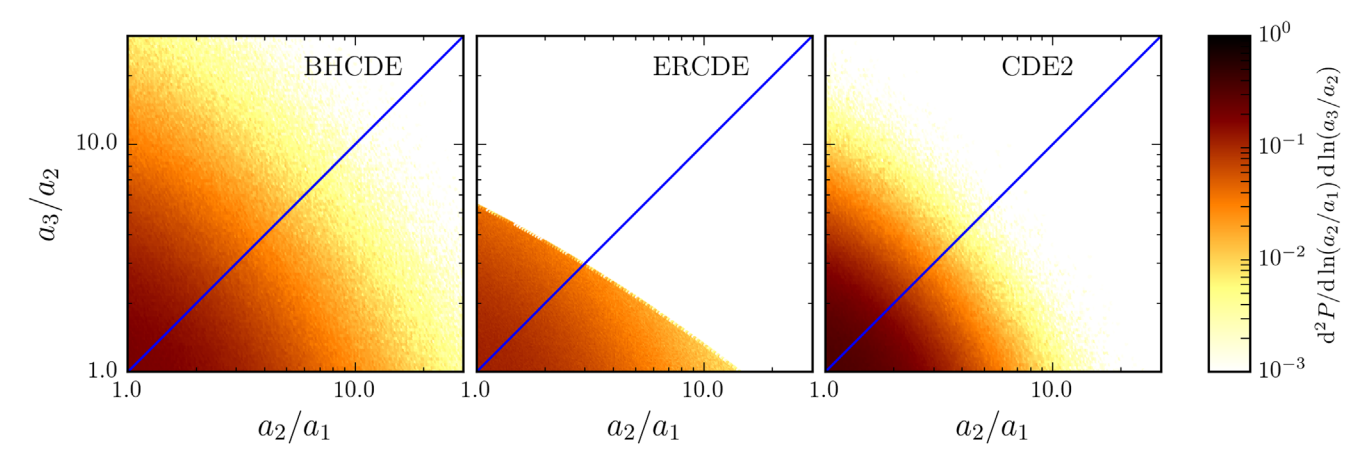


Figure 5. Distributions of axial ratios  $a_3/a_2$  and  $a_2/a_1$  for the BHCDE, ERCDE ( $L_{\min}=0.05$ ), and CDE2 shape distributions. Oblate spheroids have  $a_3/a_2=1$ , and prolate spheroids have  $a_2/a_1=1$ .

**Table 1** Long/Short Axis Ratio  $a_3/a_1$ 

	Ε,	5/ 1	
	BHCDE	ERCDE <sup>a</sup>	CDE2
Mode <sup>b</sup>	3.26	3.27	2.24
Median	4.58	3.35	2.73
25%	9.23	5.07	4.25
10%	19.7	6.97	6.72
5%	32.97	8.32	9.11
1%	98.49	10.92	17.11

#### Notes.

<sup>a</sup>  $L_{\min} = 0.05$ .

spun-up by strong radiative torques (Silsbee & Draine 2016; Hoang 2019) or gas-grain streaming (e.g., Tatsuuma & Kataoka 2021). The actual shape distribution for interstellar

grains is of course unknown, but it seems unlikely to include as large a fraction of extreme aspect ratios as the BHCDE distribution. The CDE2 (with ~90% of the draws having  $a_3/a_1 < 6.72$ ) or ERCDE (with ~90% of the draws having  $a_3/a_1 < 6.9$  for  $L_{\rm min} = 0.05$ ) may be more plausible shape distributions to consider for interstellar dust grains.

# 4. Polarization by CDEs

The observed polarization of starlight by dust, and of submillimeter emission from dust in the interstellar medium, indicates that interstellar grains spin with their short axis tending to be aligned with the local magnetic field B; this occurs because the grain's angular momentum J tends to align with the magnetic field, and the short axis of the grain tends to align with J. Rotation and nutation, and precession of J around B, are all rapid, and physical processes such as paramagnetic dissipation cause J to align with B.

<sup>&</sup>lt;sup>b</sup> Maximum of  $dP/d \ln(a_3/a_1)$ .

In protoplanetary disks, magnetic effects are relatively much weaker. Grain drift can cause J to tend to be perpendicular to the (azimuthal) streaming direction (Gold 1952), while radiative torques may cause J to tend toward the radial direction (Lazarian & Hoang 2007; Tazaki et al. 2017). Whatever the spin-up process, if the grains are spinning suprathermally we expect dissipation in the grain to cause the short axis to be aligned with J. The results obtained below for absorption cross sections averaged over CDEs are applicable both to the interstellar medium and to protoplanetary disks. This is true also for the polarization cross sections, provided only that the degree of alignment of the short axis with J is independent of shape. Interpretation of observed polarization is often complicated by the need to include polarized scattering, which can even be important at submillimeter wavelengths in protoplanetary disks (Kataoka et al. 2015).

In order to discuss polarization by a population of partially aligned grains, we require the distribution of depolarization factors separately for the short axis, and for the other two axes.

It is useful to restrict consideration to the ordering  $0 \leqslant L_3 \leqslant L_2 \leqslant L_1 \leqslant 1$ : for each ellipsoid, j=3 corresponds to the long axis, j=1 to the short axis, and j=2 to the intermediate axis. Let  $g_j(\ell)d\ell$  be the fraction of ellipsoids with  $L_j \in [\ell, \ell+d\ell]$ . The distribution functions  $g_1, g_2, g_3$  can be obtained from G, as discussed in Appendix A. Figure 6 shows  $g_1, g_2$ , and  $g_3$  for the BHCDE, ERCDE, and CDE2 shape distributions.

#### 4.1. The BHCDE Distribution

Figure 6(a) shows the distribution functions  $g_j$  for the BHCDE distribution. We see that  $g_3(\ell)$  peaks at  $\ell=0$ , corresponding to infinitely elongated needles: fully 10% of the BHCDE ellipsoids have  $L_3 < 0.0171$ . Only very extreme shapes have such small values of  $L_3$ , for example, a prolate spheroid with axial ratios 1: 1: 11.17 has  $L_3=0.0171$ . Another example with  $L_3=0.0171$  would be an ellipsoid with axial ratios 1: 4.72: 22.3. It does not seem likely (to us) that interstellar grains will have such a large fraction of extremely elongated shapes.

#### 4.2. The ERCDE Distribution

The ERCDE distribution is similar to the BHCDE distribution, except that cases with  $L < L_{\rm min}$  are excluded. Thus  $L_{\rm min}$  is a free parameter for the ERCDE distribution. The ERCDE distribution has  $g_3$  peaking at  $L_3 = L_{\rm min}$ . As an example, we consider  $L_{\rm min} = 0.05$  (see Figure 6(b)).

What shapes would correspond to the limiting cases  $L_3 = L_{\min}$ ? One example of a shape with  $L_3 = 0.05$ : a prolate spheroid with axial ratios 1:1:5.41 (with  $L_1 = L_2 = 0.475$ ,  $L_3 = 0.05$ ). Another example: an oblate spheroid with axial ratios 1:14.43:14.43 (with  $L_1 = 0.9$ ,  $L_2 = L_3 = 0.05$ ). A third example: an ellipsoid with axial ratios 1:2.965:8.79 (with  $L_1 = 0.719$ ,  $L_2 = 0.231$ ,  $L_3 = 0.05$ ).

Because  $g_3$  increases monotonically as  $L_3 \rightarrow L_{\rm min}$  (see Figure 6(b)), this shape distribution places substantial weight on the most extreme allowed grain shapes. For instance, fully 10% of the ERCDE realizations with  $L_{\rm min}=0.05$  have  $L_3 < 0.06454$ . Thus the ERCDE shape distribution also appears to overrepresent extreme shapes, unless  $L_{\rm min} \gtrsim 0.10$ . The ERCDE shape distribution will be further discussed below.

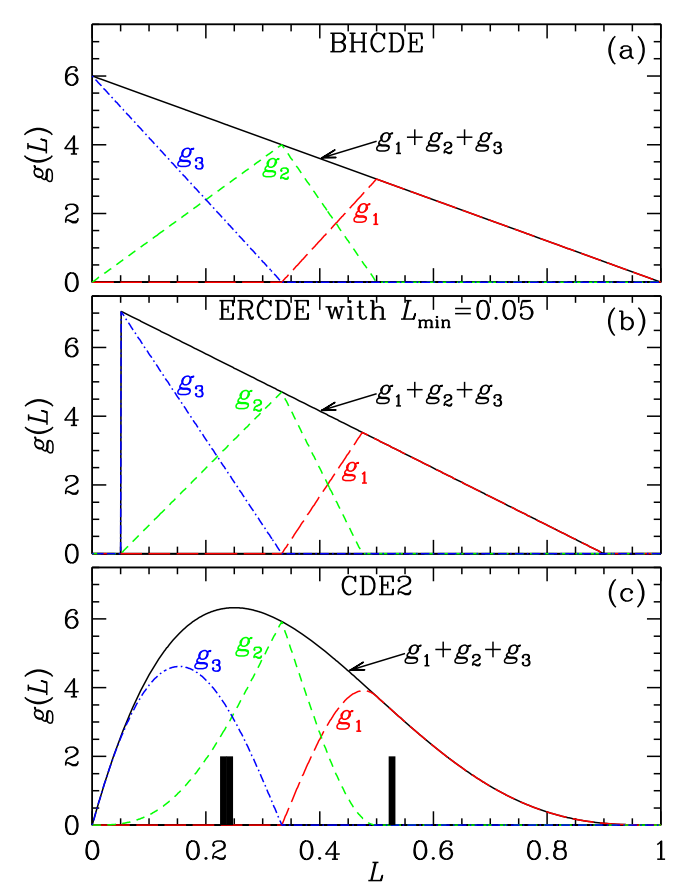


**Figure 6.** Distributions  $g_1$ ,  $g_2$ , and  $g_3$  of depolarization factors  $L_1$ ,  $L_2$ ,  $L_3$  for the three CDE distributions discussed in Section 3: (a) Bohren & Huffman CDE (BHCDE) from Equation (20). (b) Externally restricted CDE (ERCDE) from Equation (21) with  $L_{\min} = 0.05$ . (c) Ossenkopf, Henning, and Mathis CDE (CDE2) from Equation (22). The BHCDE and ERCDE distributions have extreme representation of small L. Of the three, the CDE2 distribution appears most realistic (see text). The solid bars in panel (c) show the values of  $L_3 = L_2 = 0.2364$  and  $L_1 = 0.5272$  for a b/a = 2 oblate spheroid.

#### 4.3. The CDE2 Distribution

The distribution functions  $g_j$  for the CDE2 distribution are shown in Figure 6(c). While the CDE2 does include extreme shapes, it has  $g_3 \rightarrow 0$  for  $L_3 \rightarrow 0$ , and  $g_1 \rightarrow 0$  for  $L_1 \rightarrow 1$ . Ten percent of the realizations have  $L_3 < 0.06185$ , so it is somewhat similar to the ERCDE with  $L_{\min} = 0.05$  in the representation of extreme shapes, although the CDE2 distribution function has the virtue of smoothness.

# 5. Absorption Cross Sections for the BHCDE, ERCDE and CDE2 Distributions

The shape-averaged absorption cross section associated with axis j is

$$C_{\text{abs}}(\mathbf{E}||\hat{\mathbf{a}}_{j}) = \frac{2\pi V}{\lambda} \operatorname{Im}(\langle A_{j} \rangle)$$
 (23)

$$\langle A_j \rangle \equiv \int A_j \, g_j(\ell) \, d\ell,$$
 (24)

where  $A_j$  is related to the complex dielectric function  $\epsilon$  through Equation (1). For ellipsoids with specified axial ratios  $a_1$ :  $a_2$ :  $a_3$ , the  $g_j$  are  $\delta$ -functions. As seen above, for a population of ellipsoids

with a continuous distribution of shapes, the  $g_j$  become continuous distribution functions (see Figure 6). Min et al. (2006) show that a single particle with an irregular shape also has its absorption cross section given by Equation (23) with continuous distribution functions  $g_j$ .

#### 5.1. Randomly Oriented Particles

For randomly oriented particles, the absorption cross section is

$$C_{\text{ran}} = \frac{2\pi V}{\lambda} \operatorname{Im} \left[ \frac{\langle A_1 \rangle + \langle A_2 \rangle + \langle A_3 \rangle}{3} \right]. \tag{25}$$

Bohren & Huffman (1983) obtained the absorption cross section for randomly oriented grains with the BHCDE shape distribution:

$$\frac{C_{\text{ran}}^{\text{bhcde}}}{V} = \frac{4\pi}{\lambda} \operatorname{Im} \left[ \left( \frac{1+x}{x} \right) \ln \epsilon \right], \tag{26}$$

where  $x \equiv \epsilon - 1$ . For the ERCDE (Equation (21)) the absorption cross section for randomly oriented grains was obtained by Zubko et al. (1996):

$$\frac{C_{\text{ran}}^{\text{ercde}}}{V} = \frac{4\pi}{\lambda} \frac{1}{(1 - 3L_{\text{min}})^2} \text{Im}$$

$$\times \left\{ \left( \frac{1}{x} + D \right) \ln \left[ \frac{1 + xD}{1 + xL_{\text{min}}} \right] \right\}, \tag{27}$$

where  $D \equiv 1 - 2L_{\min}$ . It is easily verified that this reduces to Equation (26) for  $L_{\min} \rightarrow 0$ .

Fabian et al. (2001) obtained the absorption cross section for randomly oriented ellipsoids with the CDE2 shape distribution (Equation (22)):

$$\frac{C_{\text{ran}}^{\text{cde2}}}{V} = \frac{40\pi}{\lambda} \text{Im}$$

$$\left[ \frac{1}{x^4} \left( -(1+x)^3 \ln(1+x) + x + \frac{5}{2}x^2 + \frac{11}{6}x^3 + \frac{1}{4}x^4 \right) \right].$$
(28)

5.2. Polarization Cross Sections for Aligned Particles
The polarization cross section (see Equation (12)) is

$$C_{\text{pol}} \equiv \frac{\pi V}{\lambda} \operatorname{Im} \times \left[ \frac{\langle A_2 \rangle + \langle A_3 \rangle - 2 \langle A_1 \rangle}{2} \right]. \tag{29}$$

For the BHCDE distribution, we find

$$\frac{C_{\text{pol}}^{\text{bhde}}}{V} = \frac{3\pi}{2\lambda} \operatorname{Im}$$

$$\times \left[ \frac{12}{x} \left( 1 + \frac{x}{2} \right) \ln \left( 1 + \frac{x}{2} \right) - \frac{9}{x} \left( 1 + \frac{x}{3} \right) \ln \left( 1 + \frac{x}{3} \right) \right]$$

$$- \frac{2}{x} (1+x) \ln (1+x) . \tag{30}$$

where  $x \equiv \epsilon - 1$ . For the ERCDE distribution we find

$$\frac{C_{\text{pol}}^{\text{ercde}}}{V} = \frac{3\pi}{2\lambda} \frac{1}{(1 - 3L_{\text{min}})^2} \times \text{Im} \left\{ 12 \left( \frac{1}{x} + B \right) \ln[1 + xB] - 9 \left( \frac{1}{x} + \frac{1}{3} \right) \ln[1 + \frac{x}{3}] - \left( \frac{1}{x} + D \right) \ln[1 + xL_{\text{min}}] - 2 \left( \frac{1}{x} + D \right) \ln[1 + xD] \right\}$$
(31)

$$B \equiv \frac{1}{2} - \frac{L_{\min}}{2}$$
 ,  $D \equiv 1 - 2L_{\min}$ . (32)

See Appendix A for the derivation of Equation (31). Equation (30) is recovered by setting  $L_{\min} = 0$ .

The polarization cross section for the CDE2 distribution is (see Appendix A):

$$\frac{C_{\text{pol}}^{\text{cde2}}}{V} = \frac{30\pi}{\lambda} \text{Im} \left[ \frac{1}{x^4} \left( 3(-9 - 3x + 3x^2 + x^3) \ln\left(1 + \frac{x}{3}\right) + 6(4 - 3x^2 - x^3) \ln\left(1 + \frac{x}{2}\right) + 2(1 + x)^3 \ln(1 + x) - 5x - \frac{1}{2}x^2 + \frac{7}{6}x^3 + \frac{11}{72}x^4 \right) \right].$$
(33)

# 6. Polarized Absorption by Partially Aligned Grains

An interstellar grain with angular momentum J will have a magnetic moment  $\mu$  resulting from a combination of the Barnett effect (if the grain has unpaired electron spins), the Rowland effect (if the grain is charged), and ferromagnetism (if the grain contains magnetic material). If  $|J \times B| \neq 0$ , the  $\mu \times B_0$  torque will cause J to precess around  $B_0$ . There are three distinct orientational issues:

- 1. The angle  $\alpha$  between the grain's principal axis of largest moment of inertia,  $\hat{a}_1$ , and the angular momentum J (alignment of the grain body with J).
- 2. The angle  $\beta$  between  $\boldsymbol{J}$  and  $\boldsymbol{B}_0$  (alignment of  $\boldsymbol{J}$  with  $\boldsymbol{B}_0$ ).
- 3. The angle  $\gamma$  between  $\boldsymbol{B}_0$  and the line of sight.

Consider radiation propagating in the  $\hat{z}$  direction, and suppose  $B_0$  to be in the  $\hat{y}$ - $\hat{z}$  plane, making an angle  $\gamma$  with the  $\hat{z}$  axis. In the electric-dipole limit  $a/\lambda \ll 1$ , the mean absorption cross section and the polarization cross section sections for x- and y-polarized radiation can be written (see Appendix B)

$$\frac{C_x + C_y}{2} = C_{\text{ran}} - C_{\text{pol}} \Phi \left( \sin^2 \gamma - \frac{2}{3} \right)$$
 (34)

$$\frac{C_x - C_y}{2} = C_{\text{pol}} \Phi \sin^2 \gamma, \tag{35}$$

where (see Appendix B)

$$\Phi = \frac{9}{4} \left( \langle \cos^2 \alpha \rangle - \frac{1}{3} \right) \left( \langle \cos^2 \beta \rangle - \frac{1}{3} \right) \tag{36}$$

<sup>&</sup>lt;sup>3</sup> For ferromagnetic grains, the rotation-averaged effective magnetic moment  $\langle \mu \rangle = J \langle J \cdot \mu \rangle / J^2$ .

is a generalization of the "polarization reduction factor" originally introduced by (Greenberg 1968, p. 328) and Purcell & Spitzer (1971). Perfect alignment ( $\langle \cos^2 \alpha \rangle = \langle \cos^2 \beta \rangle = 1$ ) has  $\Phi = 1$ ; random orientation ( $\langle \cos^2 \beta \rangle = 1/3$ ) results in  $\Phi = 0$ .

If  $B_0$  is itself not perfectly uniform, Lee & Draine (1985) showed that  $\sin^2 \gamma \rightarrow \sin^2 \gamma_0 \times \frac{3}{2} \left( \langle \cos^2 \delta \rangle - \frac{1}{3} \right)$  where  $\gamma_0$  is now the angle between  $\hat{z}$  and the (dust mass-weighted) mean magnetic field  $\langle \mathbf{B}_0 \rangle$ , and  $\delta$  is the angle between  $\langle \mathbf{B}_0 \rangle$  and the local  $B_0$ ;  $\langle \cos^2 \delta \rangle$  is the dust mass-weighted average of  $\cos^2 \delta$ over the sightline. If we assume that  $\alpha$ ,  $\beta$ , and  $\delta$  vary independently, then the overall polarization reduction factor

$$\Phi \equiv \frac{27}{8} \left( \langle \cos^2 \alpha \rangle - \frac{1}{3} \right) \left( \langle \cos^2 \beta \rangle - \frac{1}{3} \right) \left( \langle \cos^2 \delta \rangle - \frac{1}{3} \right). \tag{37}$$

Let  $N_d$  be the column density of grains, and  $C_x$  and  $C_y$  be the average absorption cross section per grain for radiation polarized in the  $\hat{x}$  and  $\hat{y}$  directions. Let  $\tau_x = N_d C_x$  and  $\tau_y = N_d C_y$  be the optical depths for radiation polarized in the  $\hat{x}$  and  $\hat{y}$  directions. Initially unpolarized radiation will be attenuated and polarized as a result of linear dichroism (i.e., preferential attenuation of one linear polarization), with overall attenuation and fractional polarization

$$I/I_0 = \frac{e^{-\tau_y} + e^{-\tau_x}}{2} \tag{38}$$

$$p = \frac{e^{-\tau_y} - e^{-\tau_x}}{e^{-\tau_y} + e^{-\tau_x}}. (39)$$

From (34) and (35) we can find the absorption cross section per grain volume  $C_{\text{ran}}(\lambda)/V$  from the measured attenuation  $I/I_0$  and polarization p (see Appendix C) where  $\rho$  is the mass density of the grain material, and  $\Sigma_d$  is the dust mass surface density:

$$\frac{C_{\text{ran}}(\lambda)}{V} = \frac{\tau_{\lambda}}{\Sigma_{\text{d}}/\rho} \left[ 1 + \frac{p_{\lambda}}{\tau_{\lambda}} \left( 1 - \frac{2}{3\sin^{2}\gamma} \right) - \frac{p_{\lambda}^{2}}{2\tau_{\lambda}} - \frac{2p_{\lambda}^{3}}{3\tau_{\lambda}} \left( 1 - \frac{2}{3\sin^{2}\gamma} \right) + O\left(\frac{p_{\lambda}^{4}}{\tau_{\lambda}}\right) \right] \tag{40}$$

Because  $p_{\lambda}/\tau_{\lambda}$  is normally small, common practice is to approximate  $C_{\rm ran}(\lambda)/V \approx \tau_{\lambda}/(\Sigma_{\rm d}/\rho)$ ; note, however, that Hensley et al. (2019) have demonstrated that the high quality of the Planck data permit the dependence of the total emission on  $p_{\lambda}/\tau_{\lambda}$  (the first-order term in Equation (40)) to be used to constrain the full 3D orientation of the magnetic field.

### 7. Self-consistent Dielectric Functions Derived from **Infrared Absorption**

The relationship between  $C_{abs}(\lambda)$  and  $C_{pol}(\lambda)$  derived in the previous sections can be leveraged on astronomical data in the infrared. Here we show how the full dielectric function  $\epsilon(\lambda)$  can be estimated using knowledge of the infrared opacity.

Suppose that we have an estimate of the dielectric function  $\epsilon(\lambda)$  of the grain material at short wavelengths  $\lambda < \lambda_1$ , and have observational knowledge of the extinction  $\tau(\lambda)$  at infrared wavelengths  $\lambda > \lambda_1$ ,  $\Sigma_d$ , and an estimate for the grain material density  $\rho$ . From these, we can estimate the observed absorption cross section per grain volume  $C_{\text{ran}}^{(\text{obs})}/V$  for randomly oriented

grains (see Appendix C). This applies to the dust material in the ISM, where we have constraints on the infrared and far-infrared opacity, including the strong silicate absorption features at 9.7 and 18  $\mu$ m. Here we show how one can use the "observed"  $C_{\rm ran}^{\rm (obs)}(\lambda)/V$  to obtain the complex dielectric function  $\epsilon(\lambda)$  at infrared wavelengths.

We assume that, at wavelengths  $\lambda > \lambda_1$ , the grains have  $a \ll \lambda$ , so that we can employ the electric-dipole approximation (8) to relate  $C_{\rm ran}/V$  to the complex dielectric function. We must, of course, make an assumption about the grain shape, or distribution of grain shapes. For spheres, spheroids, ellipsoids, or the CDEs discussed in this paper, we have analytic expressions relating  $C_{\rm ran}/V$  to the dielectric function  $\epsilon(\lambda)$ ; the analytic result enables efficient iterative algorithms to be applied to solve the system of equations.

The dielectric function must satisfy the Kramers-Kronig relations (Landau et al. 1993). We suppose that we start with a dielectric function  $\epsilon^0(\lambda)$  that is reasonably accurate at  $\lambda < \lambda_1$ . We extend the imaginary part of  $\epsilon^0$  to long wavelengths  $\lambda > \lambda_1$ in a smooth way:

$$\epsilon_2^0(\lambda) = \epsilon_2^0(\lambda_{\rm l}) \times \left(\frac{\lambda_{\rm l}}{\lambda}\right),$$
 (42)

and obtain (by numerical integration) the real part  $\epsilon_1^0(\lambda)$  at all wavelengths using the Kramers-Kronig relation (Landau et al. 1993):

$$\epsilon_1^0(\omega) = 1 + \frac{2}{\pi} P \int_0^\infty \frac{x \epsilon_2^0(x)}{x^2 - \omega^2} dx,$$
 (43)

where P indicates that the "principal value" of the singular integral is to be taken. The actual behavior of  $\epsilon_2^0(\lambda > 1 \,\mu\text{m})$  is unimportant, because we will adjust the total absorption as required to reproduce  $C_{\text{ran}}^{(\text{obs})}/V$  at  $\lambda > \lambda_1$ . We accomplish this by adding additional absorption in the form of N Lorentz oscillators, each with resonant frequency  $\omega_{0k}$ , dimensionless damping parameter  $\gamma_k$ , and dimensionless strength  $S_k$ :

$$\epsilon(\omega) = \epsilon^{(0)}(\omega) + \sum_{k=1}^{N} S_k \left[ 1 - \left( \frac{\omega}{\omega_{0k}} \right)^2 - i \gamma_k \frac{\omega}{\omega_{0k}} \right]^{-1}.$$
 (44)

Because  $\epsilon^{(0)}(\omega)$  and each of the Lorentz oscillators separately satisfy the Kramers–Kronig relations,  $\epsilon(\omega)$  given by Equation (44) will satisfy the Kramers–Kronig relations for any  $\{\omega_{0k}, \gamma_k, S_k\}$ .

We distribute the Lorentz oscillators between  $\lambda_1$  and  $\lambda_N > \lambda_1$ according to some smooth prescription (e.g., uniform in  $\log \lambda$ ). Then we set the widths of the Lorentzians by specifying the dimensionless damping parameters  $\gamma_k$ :

$$\gamma_k = C \times \left(\frac{\lambda_j}{\lambda_{j-1}} - 1\right) \text{ with } j = \max(2, k).$$
 (45)

For  $\gamma_k \ll 1$ , each resonance contributes  $\text{Im}(\epsilon)$  with a FWHM  $\approx \gamma_k \omega_{0k}$ . To represent a smooth function, we want  $\gamma_k \omega_{0k}$  to be large compared to  $\omega_{0,k+1} - \omega_{0k}$ , but small enough to be able to reproduce the expected frequency dependence of  $\operatorname{Im}(\epsilon)$ . This is accomplished by suitable choice for C. For example, Draine & Hensley (2021) adopt N=3000,  $\omega_{01}/\omega_{0N}=3$  cm/1  $\mu$ m =  $3\times10^4$ , and C=10. The model cross sections  $C_{\rm ran}^{\rm (model)}(\lambda)$  depend on the  $\{S_k\}$ . To

find the self-consistent solution, we iteratively adjust the  $S_k$  to

solve the *N* simultaneous equations

$$Y_{k} \equiv \left[\frac{\lambda C_{\text{ran}}^{(\text{model})}}{V}\right]_{\lambda_{k}} - \left[\frac{\lambda C_{\text{ran}}^{(\text{obs})}}{V}\right]_{\lambda_{k}} = 0 \quad , \quad k = 1, ..., N.$$
(46)

Thus we have N equations to determine N unknown  $S_k$ . Iterative alogrithms, such as the Levenberg-Marquardt method (see, e.g., Press et al. 1992), can be used to find the solution  $S_k$ ; it is helpful that analytic formulae for the partial derivatives  $\partial Y_j/\partial S_k$  can be obtained from Equation (44) and one of (8), (26), (27), or (28).

We remark here that the problem does not always have a solution: if the "observed"  $\lambda C_{\rm ran}^{\rm (obs)}/V$  is too large, there may not be any dielectric function  $\epsilon(\lambda)$  that can reproduce the assumed  $\lambda C_{\rm ran}^{\rm (obs)}/V$  for the assumed grain shape. Because of the Kramers–Kronig relations, all wavelengths matter: strong absorption at one wavelength will imply a large  ${\rm Re}(\epsilon)$  at longer wavelengths, limiting the ability of the grain to absorb at those wavelengths.

We apply this methodology to estimate the effective dielectric function  $\epsilon(\lambda)$  for interstellar dust material in a separate paper (Draine & Hensley 2021).

### 8. Ellipsoids versus More Complex Shapes

This paper has concentrated on the optics of grains with spheroidal or ellipsoidal shapes, including continuous distributions of ellipsoidal shapes. In the Rayleigh limit  $a \ll \lambda$ , the interaction of a grain with the electromagnetic field is determined by a single symmetric tensor  $\alpha_{jk}$  characterizing the polarizability of the grain. For a given dielectric function, ellipsoidal shapes allow us to explore plausible values for  $\alpha_{jk}/V$ .

At shorter wavelengths, the response of the grain to an incident electromagnetic field is more complex, and ellipsoidal shapes provide only a first approximation to asphericity. Ellipsoidal shapes may be an adequate approximation for estimation of cross sections for absorbing or scattering light, for modeling polarization of starlight at optical wavelengths, or polarized thermal emission at submillimeter wavelengths.

However, radiative torques are important for grain dynamics, including the alignment of interstellar grains (Draine & Weingartner 1996, 1997; Hoang & Lazarian 2008). The reflection symmetries (and therefore zero chirality) of ellipsoidal shapes artificially suppresses radiative torques. Therefore, studies of radiative torques on interstellar grains must consider non-ellipsoidal grain shapes. However, the overall deviations from nonsphericity implied by observations of polarized emission at long wavelengths will still serve to constrain the more complex shapes used for studies of starlight torques.

#### 9. Summary

The principal results of this study are as follows:

- 1. We discuss the distributions of ellipsoidal shapes that correspond to three previously proposed CDEs. Twenty randomly selected shapes from each distribution (Figure 3) serve to illustrate the three distributions.
- 2. The often-used CDE discussed by Bohren & Huffman (1983) (here referred to as the BHCDE distribution)

- includes what appears to be an unrealistically large fraction of extremely elongated or extremely flattened shapes.
- The CDE2 distribution proposed by Ossenkopf et al. (1992) includes a much smaller fraction of extreme shapes and seems more realistic as a model for distributions of grain shapes.
- 4. For each of the three CDEs considered here, we obtain the distribution functions  $g_j(L_j)$  for the geometric factors  $L_1$ ,  $L_2$ ,  $L_3$ .
- 5. In the electric-dipole limit  $a/\lambda \ll 1$ , we obtain absorption and polarization cross sections for partially aligned ellipsoidal grains with the three proposed CDEs.
- 6. We present a method for obtaining a self-consistent dielectric function consistent with an assumed absorption opacity and an assumed distribution of shapes.

We thank Eric Stansifer and Chris Wright for helpful discussions. We thank the referee for helpful comments, and also thank a previous referee for comments on an earlier version. This work was supported in part by NSF grants AST-1408723 and AST-1908123, and carried out in part at the Jet Propulsion Laboratory, California Institute of Technology, under a contract with the National Aeronautics and Space Administration.

# Appendix A Polarization Cross Sections for Grain Populations with Continuously Distributed Ellipticities

#### A.1. General Considerations

Consider a population of ellipsoids with a distribution of axial ratios. Every ellipsoidal shape is uniquely specified by its triplet of depolarization factors  $(L_1, L_2, L_3)$ . Because  $L_3 = 1 - L_1 - L_2$ , the ellipsoid is fully determined by the doublet  $(L_1, L_2)$ , which must lie in the triangular region bounded by  $L_1 = 0$ ,  $L_2 = 0$ , and  $L_1 + L_2 = 1$ , as shown in Figure 1.

The distribution of shapes can be characterized by the distribution of L values. Let  $dP = G(L_1, L_2)dL_1dL_2$  be the probability that  $L_1 \in (L_1 + dL_1)$ ,  $L_2 \in (L_2 + dL_2)$ . The function  $G(L_1, L_2)$  fully determines the shape distribution (i.e., the distribution of axial ratios). If G is to apply to the full triangular region in Figure 1, then (because labeling of axes 1, 2, 3 is arbitrary), G must depend symmetrically on  $L_1$ ,  $L_2$ ,  $L_3$ :

$$G(L_1, L_2) = G(L_2, L_1) = G(L_1, 1 - L_1 - L_2)$$
  
for all allowed  $L_1, L_2$ . (A1)

The region of allowed  $(L_1, L_2)$  can be divided into six triangular subregions of equal area, shown in Figure 1, corresponding to the six possible orderings of  $L_1, L_2, L_3$ : (1)  $L_3 \leqslant L_2 \leqslant L_1$ , (2)  $L_2 \leqslant L_1 \leqslant L_3$ , (3)  $L_1 \leqslant L_3 \leqslant L_2$ , (4)  $L_2 \leqslant L_3 \leqslant L_1$ , (5)  $L_3 \leqslant L_1 \leqslant L_2$ , and (6)  $L_1 \leqslant L_2 \leqslant L_3$ .

For clarity, we fix the order of the L values: we choose the ordering  $0 \le L_3 \le L_2 \le L_1 \le 1$ , corresponding to region 1 (shaded) in Figure 1. Then  $L_1$  is for E parallel to the principal axis of largest moment of inertia (the "short axis"), and  $L_3$  is for E along the principal axis of smallest moment of inertia (the "long axis").

Within subregion 1, let  $g_j(L_j)dL_j$  be the probability that  $L_j \in (L_j, L_j + dL_j)$ :

$$g_{1}(L_{1}) = 0 \qquad \text{for } 0 < L_{1} < 1/3$$

$$= 6 \int_{(1-L_{1})/2}^{L_{1}} G(L_{1}, L_{2}) dL_{2} \qquad \text{for } 1/3 < L_{1} < 1/2$$

$$= 6 \int_{(1-L_{1})/2}^{1-L_{1}} G(L_{1}, L_{2}) dL_{2} \qquad \text{for } 1/2 < L_{1} < 1$$

$$g_{2}(L_{2}) = 6 \int_{1-2L_{2}}^{1-L_{2}} G(L_{1}, L_{2}) dL_{1} \qquad \text{for } 0 < L_{2} < 1/3$$

$$= 6 \int_{L_{2}}^{1-L_{2}} G(L_{1}, L_{2}) dL_{1} \qquad \text{for } 1/3 < L_{2} < 1/2$$

$$= 0 \qquad \text{for } 1/2 < L_{2}$$

$$g_{3}(L_{3}) = 3 \int_{0}^{1-3L_{3}} G((1-L_{3}+z)/2, (1-L_{3}-z)/2) dz \qquad \text{for } 0 < L_{3} < 1/3$$

$$= 0 \qquad \text{for } 1/3 < L_{3} \qquad \text{(A2)}$$

where we have introduced  $z \equiv (L_1 - L_2)$  for evaluation of  $g_3$ . The factor of six in (A2) appears because we assume the normalization  $\int G dL_1 dL_2 = 1$  over the full triangular region, hence  $\int G dL_1 dL_2 = 1/6$  over region 1. It can be verified that

$$\int_0^1 g_j(L_j) dL_j = 1 \quad \text{for } j = 1, 2, 3.$$
 (A3)

For distributions of ellipsoidal shapes,

$$\langle A_j \rangle \equiv \int \frac{(\epsilon - 1)}{1 + L_i(\epsilon - 1)} g_j(L_j) dL_j.$$
 (A4)

## A.2. BHCDE

The simplest CDE is the uniform distribution

$$G(L_1, L_2) = 2$$
 for  $0 \le L_1 + L_2 \le 1$ , (A5)

which obviously satisfies the symmetry condition (A1). This example was discussed by Bohren & Huffman (1983); we refer to (A5) as the BHCDE. For this case we have

$$g_{1} = 0 for L_{1} < \frac{1}{3}$$

$$= 18(L_{1} - \frac{1}{3}) for \frac{1}{3} \le L_{1} \le \frac{1}{2}$$

$$= 6(1 - L_{1}) for \frac{1}{2} \le L_{1} \le 1$$

$$g_{2} = 12L_{2} for 0 \le L_{2} \le \frac{1}{3}$$

$$= 12(1 - 2L_{2}) for \frac{1}{3} \le L_{2} \le \frac{1}{2}$$

$$= 0 for \frac{1}{2} \le L_{2}$$

$$g_{3} = 6(1 - 3L_{3}) for 0 \le L_{3} \le \frac{1}{3}$$

$$= 0 for \frac{1}{2} \le L_{3}. (A6)$$

Distributions  $g_1$ ,  $g_2$ , and  $g_3$  are shown in Figure 6(a). Then

$$\langle A_1 \rangle = \frac{6}{x} \left\{ (1+x) \ln \left( \frac{1+x}{1+x/2} \right) - 3 \left( 1 + \frac{x}{3} \right) \ln \left( \frac{1+x/2}{1+x/3} \right) \right\}$$
(A7)

$$\langle A_2 \rangle = \frac{12}{x} \left\{ 2 \left( 1 + \frac{x}{2} \right) \ln \left( \frac{1 + x/2}{1 + x/3} \right) - \ln (1 + x/3) \right\}$$
(A8)

$$\langle A_3 \rangle = \frac{18}{x} \left\{ \left( 1 + \frac{x}{3} \right) \ln(1 + x/3) - \frac{x}{3} \right\}.$$
 (A9)

$$\frac{\langle A_1 + A_2 + A_3 \rangle}{3} = \frac{2}{x} (1+x) \ln(1+x) - 2. \tag{A10}$$

Equation (A10) was previously obtained by Bohren & Huffman (1983).

#### A.3. ERCDE

The BHCDE includes shapes that are infinitely elongated  $(L_j \rightarrow 0)$  and infinitely flattened  $(L_j \rightarrow 1)$ . Zubko et al. (1996) proposed to exclude the most extreme shapes by imposing the restriction  $L_j \geqslant L_{\min}$ , where  $0 \leqslant L_{\min} \leqslant 1/3$ , giving what Zubko et al. referred to as the "externally restricted distribution of ellipsoids" (ERCDE):

$$G(L_1, L_2) = \frac{2}{(1 - 3L_{\min})^2} \text{ for}$$

$$L_{\min} \leq L_1, \ L_{\min} \leq L_2,$$

$$(L_1 + L_2) \leq 1 - 2L_{\min}. \tag{A11}$$

With  $L_{\min} = 0$  one obtains the original BHCDE; with  $L_{\min} \rightarrow 1/3$  one obtains spheres. The domain in the  $L_1$ – $L_2$  plane is shown in Figure 7.

Zubko et al. (1996) obtained  $\langle A_1 + A_2 + A_3 \rangle$  for randomly oriented grains with the ERCDE distribution. Discussion of aligned grains requires the absorption per volume for grains aligned with the electric fields along their principal axes. The ERCDE has

$$g_{1} = 0 \qquad \text{for } L_{1} < \frac{1}{3}$$

$$= \frac{18}{(1 - 3L_{\min})^{2}} \left( L_{1} - \frac{1}{3} \right) \qquad \text{for } \frac{1}{3} \leqslant L_{1} \leqslant \frac{(1 - L_{\min})}{2}$$

$$= \frac{6}{(1 - 3L_{\min})^{2}} (1 - L_{1} - 2L_{\min}) \text{ for } \frac{(1 - L_{\min})}{2} \leqslant L_{1} \leqslant 1 - 2L_{\min}$$

$$= 0 \qquad \text{for } 1 - 2L_{\min} \leqslant L_{1}$$

$$g_{2} = 0 \qquad \text{for } L_{2} < L_{\min}$$

$$= \frac{12}{(1 - 3L_{\min})^{2}} (L_{2} - L_{\min}) \qquad \text{for } L_{\min} \leqslant L_{2} \leqslant \frac{1}{3}$$

$$= \frac{12}{(1 - 3L_{\min})^{2}} (1 - L_{\min} - 2L_{2}) \text{ for } \frac{1}{3} \leqslant L_{2} \leqslant \frac{(1 - L_{\min})}{2}$$

$$= 0 \qquad \text{for } \frac{(1 - L_{\min})}{2} \leqslant L_{2}$$

$$g_{3} = 0 \qquad \text{for } L_{3} \leqslant L_{\min}$$

$$= \frac{6}{(1 - 3L_{\min})^{2}} (1 - 3L_{3}) \qquad \text{for } L_{\min} \leqslant L_{3} \leqslant \frac{1}{3}$$

$$= 0 \qquad \text{for } \frac{1}{3} \leqslant L_{3}. \qquad (A12)$$

Distributions  $g_1$ ,  $g_2$ , and  $g_3$  are shown in Figure 6(b) for  $L_{\min} = 0.05$ . It is convenient to define

$$B \equiv 1/2 - L_{\min}/2 \tag{A13}$$

$$D \equiv 1 - 2L_{\min} \tag{A14}$$

$$x \equiv \epsilon - 1. \tag{A15}$$

We obtain

$$\langle A_{1} \rangle = \frac{6}{(1 - 3L_{\min})^{2}} \left\{ \left( \frac{1}{x} + D \right) \ln \left[ \frac{1 + xD}{1 + xB} \right] - 3 \left( \frac{1}{x} + \frac{1}{3} \right) \ln \left[ \frac{1 + xB}{1 + x/3} \right] \right\}$$

$$\langle A_{2} \rangle = \frac{12}{(1 - 3L_{\min})^{2}} \left\{ 2 \left( \frac{1}{x} + B \right) \ln \left[ \frac{1 + xB}{1 + x/3} \right] - \left( \frac{1}{x} + L_{\min} \right) \ln \left[ \frac{1 + x/3}{1 + xL_{\min}} \right] \right\}$$
(A16)

$$\langle A_3 \rangle = \frac{18}{(1 - 3L_{\min})^2} \left\{ \left( \frac{1}{x} + \frac{1}{3} \right) \times \ln \left[ \frac{1 + x/3}{1 + xL_{\min}} \right] - \frac{(1 - 3L_{\min})}{3} \right\}$$
(A18)

$$\frac{\langle A_1 + A_2 + A_3 \rangle}{3} = \frac{2}{(1 - 3L_{\min})^2} \times \left\{ \left( \frac{1}{x} + D \right) \ln \left[ \frac{1 + xD}{1 + xL_{\min}} \right] - (1 - 3L_{\min}) \right\}.$$
(A19)

Equation (A19) was previously obtained by Zubko et al. (1996).

#### A.4. CDE2

Ossenkopf et al. (1992) proposed the distribution

$$G(L_1, L_2) = 120L_1L_2L_3.$$
 (A20)

This satisfies the symmetry requirement (A1), and has the desirable property that  $G \rightarrow 0$  for  $L_j \rightarrow 0$ . We find

$$g_{1}(L_{1}) = 0 \qquad \text{for } L_{1} < \frac{1}{3}$$

$$= 60L_{1}(-1 + 3L_{1} + 3L_{1}^{2} - 9L_{1}^{3})\text{for } \frac{1}{3} \le L_{1} \le \frac{1}{2}$$

$$= 60L_{1}(1 - L_{1})^{3} \qquad \text{for } \frac{1}{2} \le L_{1} \le 1$$

$$g_{2}(L_{2}) = 120L_{2}^{3}(3 - 5L_{2}) \qquad \text{for } 0 \le L_{2} \le \frac{1}{3}$$

$$= 120(L_{2} - 3L_{2}^{2} + 4L_{2}^{4}) \qquad \text{for } \frac{1}{3} \le L_{2} \le \frac{1}{2}$$

$$= 0 \qquad \text{for } \frac{1}{2} < L_{2}$$

$$g_{3}(L_{3}) = 60L_{3}(1 - 3L_{3} - 3L_{3}^{2} + 9L_{3}^{3}) \quad \text{for } 0 \le L_{3} \le \frac{1}{3}$$

$$= 0 \qquad \text{for } \frac{1}{3} < L_{3}.$$

$$(A21)$$

These distributions are shown in Figure 6(c). To have a sense of how nonspherical a typical ellipsoid from this distribution might be, we consider the mean depolarization factors  $\langle L_j \rangle \equiv \int L_j g_j(L_j) dL_j$ . For  $g_j$  given by Equation (A21), we find  $\langle L_1 \rangle = 0.5355$ ,  $\langle L_2 \rangle = 0.3040$ , and  $\langle L_3 \rangle = 0.1605$ . These mean values correspond to an ellipsoid with axial ratios  $a_1$ :  $a_2$ :  $a_3$ ::1: 1.664: 2.716.

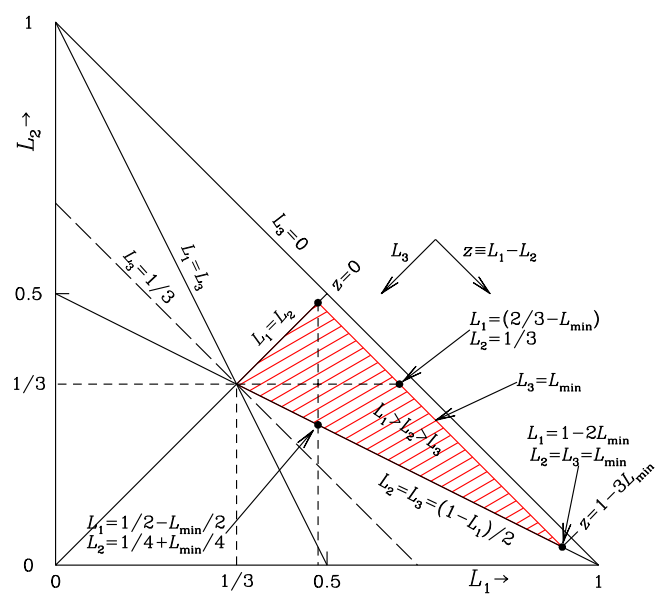


**Figure 7.** The shaded area is the ERCDE locus with depolarization factors  $L_1 \geqslant L_2 \geqslant L_3 \geqslant L_{\min}$  (see text).

For  $g_i$  given by Equation (A21), we obtain

$$\langle A_1 \rangle = \frac{60}{x^4} \left[ (9 + 3x - 3x^2 - x^3) \right]$$

$$\ln\left(1 + \frac{x}{3}\right) + (-8 + 6x^2 + 2x^3) \ln\left(1 + \frac{x}{2}\right)$$

$$+ (-1 - 3x - 3x^2 - x^3) \ln(1 + x)$$

$$+ 2x + x^2 + \frac{2}{9}x^3 + \frac{7}{216}x^4 \right] \qquad (A22)$$

$$\langle A_2 \rangle = \frac{60}{x^4} \left[ (-18 - 6x + 6x^2 + 2x^3) \ln\left(1 + \frac{x}{3}\right) + (8 - 6x^2 - 2x^3) \ln\left(1 + \frac{x}{2}\right) + 2x + 2x^2 + \frac{5}{9}x^3 + \frac{13}{216}x^4 \right] \qquad (A23)$$

$$\langle A_3 \rangle = \frac{60}{x^4} \left[ (9 + 3x - 3x^2 - x^3) \ln\left(1 + \frac{x}{3}\right) - 3x - \frac{1}{2}x^2 + \frac{19}{18}x^3 + \frac{17}{108}x^4 \right] \qquad (A24)$$

$$\frac{\langle A_1 + A_2 + A_3 \rangle}{3} = \frac{20}{x^4}$$

$$\times \left[ -(1 + x)^3 \ln(1 + x) + x + \frac{5}{2}x^2 + \frac{11}{6}x^3 + \frac{1}{4}x^4 \right], \qquad (A25)$$

where  $x \equiv \epsilon - 1$ . Equation (A25) was previously obtained by Fabian et al. (2001).

# Appendix B Orientation-averaged Cross Sections for Partially Aligned Grains

Consider radiation propagating along the  $\hat{z}$  axis. Let the local magnetic field be in the  $\hat{y} - \hat{z}$  plane, with  $\gamma =$  the angle

between  $\hat{\pmb{B}}$  and the line of sight:  $\hat{\pmb{B}} = \hat{\pmb{y}} \sin \gamma + \hat{\pmb{z}} \cos \gamma$ . Let  $\hat{\pmb{J}}$  be a unit vector in the direction of the grain's angular momentum, and  $\beta$  the angle between  $\hat{\pmb{J}}$  and  $\hat{\pmb{B}}$ . If  $\beta > 0$ , the grain's magnetic moment will cause  $\hat{\pmb{J}}$  to precess around  $\hat{\pmb{B}}$ , and we may write

$$\hat{\boldsymbol{J}} = \hat{\boldsymbol{B}}\cos\beta + \hat{\boldsymbol{x}}\sin\beta\cos\phi_1 + (\hat{\boldsymbol{x}}\times\hat{\boldsymbol{B}})\sin\beta\sin\phi_1 \quad (B1)$$

$$= \hat{\mathbf{x}} \sin \beta \cos \phi_1 + \hat{\mathbf{y}} (\cos \beta \sin \gamma - \sin \beta \cos \gamma \sin \phi_1) + \hat{\mathbf{z}} (\cos \beta \cos \gamma + \sin \beta \sin \gamma \sin \phi_1),$$
 (B2)

with  $\phi_1$  varying from 0 to  $2\pi$  over one precession period. Observations of starlight polarization indicate that there is systematic alignment of J with B, i.e.,  $\langle \cos^2 \beta \rangle > 1/3$ , with the alignment presumed to result from some combination of paramagnetic dissipation (Davis & Greenstein 1951), superparamagnetic dissipation (Jones & Spitzer 1967), ferromagnetic dissipation (Draine & Hensley 2013), or starlight torques (Draine & Weingartner 1997; Weingartner & Draine 2003; Hoang & Lazarian 2009a, 2009b).

On short timescales, the grain spins and nutates with fixed  $\hat{J}$  according to the dynamics of rigid bodies (see, e.g., Weingartner & Draine 2003). Let  $\hat{a}_1$  be the principal axis of largest moment of inertia, and let  $\alpha$  be the angle between  $\hat{J}$  and  $\hat{a}_1$ . At constant J and kinetic energy  $E_{\rm rot}$  the grain will tumble:  $\hat{a}$  will nutate around  $\hat{J}$ . If the grain is triaxial, the angle  $\alpha$  does not remain constant during the nutation, but will have some time-averaged value of  $\langle \cos^2 \alpha \rangle$ .

For fixed J, the kinetic energy of the grain is minimized if  $\alpha = 0$  ( $\cos^2 \alpha = 1$ ). If the direction of  $\hat{a}$  is uncorrelated with  $\hat{J}$ , then  $\langle \cos^2 \alpha \rangle = 1/3$ . Thus we expect dissipation in the grain to result in  $\langle \cos^2 \alpha \rangle > 1/3$ . Suprathermally rotating grains, with rotational kinetic energy  $E_{\rm rot} \gg kT_{\rm grain}$ , are expected to have  $\cos^2 \alpha \approx 1$  as the result of dissipation associated with viscoelasticity (Purcell 1979) or the even greater dissipation associated with the Barnett effect (Lazarian & Roberge 1997) and nuclear spin relaxation (Lazarian & Draine 1999).

After averaging over precession and nutation,

$$\langle (\hat{\boldsymbol{a}}_1 \cdot \hat{\boldsymbol{x}})^2 \rangle = \frac{1}{3} - \frac{3}{4} \left( \langle \cos^2 \alpha \rangle - \frac{1}{3} \right)$$
$$\times \left( \cos^2 \beta - \frac{1}{3} \right) \tag{B3}$$

$$\langle (\hat{\mathbf{a}}_1 \cdot \hat{\mathbf{y}})^2 \rangle = \frac{1}{3} + \frac{9}{4} \left( \langle \cos^2 \alpha \rangle - \frac{1}{3} \right)$$
$$\times \left( \cos^2 \beta - \frac{1}{3} \right) \left( \sin^2 \gamma - \frac{1}{3} \right) \tag{B4}$$

$$\langle (\hat{a}_2 \cdot \hat{x})^2 \rangle = \langle (\hat{a}_3 \cdot \hat{x})^2 \rangle = \frac{1}{3} + \frac{3}{8}$$
$$\times \left( \langle \cos^2 \alpha \rangle - \frac{1}{3} \right) \left( \langle \cos^2 \beta \rangle - \frac{1}{3} \right) \tag{B5}$$

$$\langle (\hat{\boldsymbol{a}}_2 \cdot \hat{\boldsymbol{y}})^2 \rangle = \langle (\hat{\boldsymbol{a}}_3 \cdot \hat{\boldsymbol{y}})^2 \rangle = \frac{1}{3} - \frac{9}{8} \times \left( \langle \cos^2 \alpha \rangle - \frac{1}{3} \right) \left( \sin^2 \gamma - \frac{1}{3} \right).$$
(B6)

The cross sections for radiation polarized in the  $\hat{x}$  and  $\hat{y}$  directions are

$$C_x = C_{\text{ran}} + \frac{2}{3}C_{\text{pol}}\Phi \tag{B7}$$

$$C_{y} = C_{\text{ran}} - 2C_{\text{pol}}\Phi\left(\sin^{2}\gamma - \frac{1}{3}\right)$$
 (B8)

$$\frac{C_x + C_y}{2} = C_{\text{ran}} - C_{\text{pol}} \Phi \left( \sin^2 \gamma - \frac{2}{3} \right)$$
 (B9)

$$\frac{C_x - C_y}{2} = C_{\text{pol}} \Phi \sin^2 \gamma \tag{B10}$$

$$C_{\text{ran}} \equiv \frac{1}{3} [C_{\text{abs}}(E \| \hat{a}_1) + C_{\text{abs}}(E \| \hat{a}_2) + C_{\text{abs}}(E \| \hat{a}_3)]$$
 (B11)

$$C_{\text{pol}} \equiv \frac{1}{4} [C_{\text{abs}}(E \| \hat{a}_2) + C_{\text{abs}}(E \| \hat{a}_3) - 2C_{\text{abs}}(E \| \hat{a}_1)] \quad (B12)$$

$$\Phi \equiv \frac{9}{4} \left( \langle \cos^2 \alpha \rangle - \frac{1}{3} \right) \left( \cos^2 \beta - \frac{1}{3} \right). \tag{B13}$$

# Appendix C Estimating $C_{\text{ran}}$ from Observations

Suppose that the attenuation  $I/I_0$  is known, where the intensity  $I(\lambda)$  is summed over both polarization modes, and the unattenuated radiation  $I_0$  is unpolarized. The fractional polarization  $p(\lambda)$  is also measured. Let  $\hat{z}$  be the direction of propagation, and  $\hat{y}$  be the polarization direction. If N is the total column density of grains, we seek to determine the cross section  $C_{\rm ran}(\lambda)$  for randomly oriented grains. Define

$$\bar{\tau} \equiv \frac{\tau_x + \tau_y}{2} \tag{C1}$$

$$\tau_p \equiv \frac{\tau_x - \tau_y}{2}.$$
 (C2)

Then

$$\frac{I}{I_0} = \frac{e^{-\tau_x} + e^{-\tau_y}}{2} \tag{C3}$$

$$=e^{-\bar{\tau}} \left[ 1 - \frac{1}{2} \tau_p^2 + O(\tau_p^4) \right]. \tag{C4}$$

$$p = \frac{e^{-\tau_y} - e^{-\tau_x}}{2I/I_0}$$
 (C5)

$$=\tau_p \frac{\left[1 + \frac{1}{6}\tau_p^2 + O(\tau_p^4)\right]}{\left[1 - \frac{1}{2}\tau_p^2 + O(\tau_p^4)\right]} = \tau_p \left[1 + \frac{2}{3}\tau_p^2 + O(\tau_p^4)\right], \quad (C6)$$

$$\tau_p \approx p - \frac{2}{3}p^3 + O(p^5),\tag{C7}$$

$$\bar{\tau} = \ln(I_0/I) + \ln\left[1 - \frac{1}{2}\tau_p^2 + O(\tau_p^4)\right]$$
 (C8)

$$\approx \ln(I_0/I) - \frac{1}{2}\tau_p^2 + O(\tau_p^4)$$
 (C9)

$$\approx \ln(I_0/I) - \frac{1}{2}p^2 + O(p^4).$$
 (C10)

From (B9)–(B12), we have

$$\bar{\tau} = N \left[ C_{\text{ran}} - C_{\text{pol}} \Phi \left( \sin^2 \gamma - \frac{2}{3} \right) \right]$$
 (C11)

$$=NC_{\rm ran} - \tau_p \left(1 - \frac{2}{3\sin^2\gamma}\right). \tag{C12}$$

Using (C7) and (C10), we obtain

$$C_{\text{ran}} = \frac{1}{N} \left[ \ln \left( \frac{I_0}{I} \right) + p \left( 1 - \frac{2}{3 \sin^2 \gamma} \right) - \frac{1}{2} p^2 - \frac{2}{3} p^3 \left( 1 - \frac{2}{3 \sin^2 \gamma} \right) + O(p^4) \right]. \quad (C13)$$

If the polarization fraction  $p \ll 1$ , we may approximate  $C_{\text{ran}} \approx (1/N) \ln(I_0/I)$ . For finite  $p \lesssim 0.2$ , we can correct for the alignment if p is measured and  $\sin^2 \gamma$  can be estimated.

# Appendix D Proof of Uniqueness

For an ellipsoid with semimajor axes  $a_1 \le a_2 \le a_3$ , the corresponding shape factors  $L_1 \ge L_2 \ge L_3$  are given by Equations (2) and (3). While we do not offer a proof that there is an  $(a_2/a_1, a_3/a_1)$  corresponding to every possible  $(L_1, L_2, L_3)$ , we have implemented a numerical procedure that always returns a solution. In this note, we demonstrate that this solution is unique.

Suppose that  $(a_2/a_1, a_3/a_1)$  corresponds to the desired  $(L_1, L_2, L_3)$ . Without loss of generality, let  $a_1 = 1$ . We may then rewrite

$$L_{j} = \frac{a_{2}a_{3}}{2} \int_{0}^{\infty} \frac{dx}{(a_{j}^{2} + x)[(1 + x)(a_{2}^{2} + x)(a_{3}^{2} + x)]^{1/2}}.$$
(D1)

Computing the derivatives

$$\frac{\partial L_1}{\partial a_2} = \frac{1}{2} \int_0^\infty \frac{a_3 x dx}{(1+x)^{3/2} (a_2^2 + x)^{3/2} (a_3^2 + x)^{1/2}}$$
 (D2)

$$\frac{\partial L_1}{\partial a_3} = \frac{1}{2} \int_0^\infty \frac{a_2 x dx}{(1+x)^{3/2} (a_2^2 + x)^{1/2} (a_3^2 + x)^{3/2}}$$
 (D3)

$$\frac{\partial L_2}{\partial a_3} = \frac{1}{2} \int_0^\infty \frac{a_2 x dx}{(1+x)^{1/2} (a_2^2 + x)^{3/2} (a_3^2 + x)^{3/2}}$$
 (D4)

$$\frac{\partial L_3}{\partial a_2} = \frac{1}{2} \int_0^\infty \frac{a_3 x dx}{(1+x)^{1/2} (a_2^2 + x)^{3/2} (a_3^2 + x)^{3/2}}, \quad (D5)$$

we see that the integrands are positive definite for all  $a_2$ ,  $a_3$ , and x. Therefore,

$$\frac{\partial L_1}{\partial a_2} > 0$$
,  $\frac{\partial L_1}{\partial a_3} > 0$ ,  $\frac{\partial L_2}{\partial a_3} > 0$ ,  $\frac{\partial L_3}{\partial a_2} > 0$ . (D6)

Because the  $L_i$  sum to one, it must be true that

$$\frac{\partial L_1}{\partial a_2} + \frac{\partial L_2}{\partial a_2} + \frac{\partial L_3}{\partial a_2} = 0 \tag{D7}$$

$$\frac{\partial L_1}{\partial a_3} + \frac{\partial L_2}{\partial a_3} + \frac{\partial L_3}{\partial a_3} = 0,$$
 (D8)

and so

$$\frac{\partial L_2}{\partial a_2} < 0, \quad \frac{\partial L_3}{\partial a_3} < 0.$$
 (D9)

Assume that there are two sets of axial ratios  $(a_2, a_3)$  and  $(a_2', a_3')$  that yield the same  $(L_1, L_2, L_3)$ . We will proceed by starting from  $(a_2, a_3)$  and adjusting the axial ratios one at a time to the values  $(a_2', a_3')$ . We will show that it is impossible to make a nonzero adjustment and return back to the original  $(L_1, L_2, L_3)$ . Note that, since  $1 \le a_2 \le a_3$  by construction,  $L_1 \ge L_2 \ge L_3$  and thus permutations of the  $L_i$  are excluded.

If  $a_2 > a_2'$ , we can first decrease  $a_2$  until it is equal to  $a_2'$ . From the relations above, doing so decreases  $L_1$ , increases  $L_2$ , and decreases  $L_3$ . To return the  $L_j$  to their original values, adjusting  $a_3$  must increase  $L_1$ , decrease  $L_2$ , and increase  $L_3$ . However, decreasing  $a_3$  decreases  $L_1$  while increasing  $a_3$  increases  $L_2$ , and so the desired adjustment is not possible. An analogous argument holds for  $a_2 < a_2'$ .

Therefore,  $(a_2, a_3)$  is the *unique* set of axial ratios corresponding to  $(L_1, L_2, L_3)$ .

#### ORCID iDs

B. T. Draine https://orcid.org/0000-0002-0846-936X Brandon S. Hensley https://orcid.org/0000-0001-7449-4638

#### References

```
Alexander, D. B., & Ferguson, J. W. 1994, in IAU Coll. 146, Molecules in the Stellar Environment, ed. U. G. Jorgensen (Berlin: Springer), 149
Altobelli, N., Postberg, F., Fiege, K., et al. 2016, Sci, 352, 312
Bohren, C. F., & Huffman, D. R. 1983, Absorption and Scattering of Light by Small Particles (New York: Wiley)
Davis, L. J., & Greenstein, J. L. 1951, ApJ, 114, 206
Draine, B. T., & Hensley, B. 2013, ApJ, 765, 159
Draine, B. T., & Hensley, B. S. 2021, ApJ, 909, 94
Draine, B. T., & Lee, H. M. 1984, ApJ, 285, 89
```

Draine, B. T., & Weingartner, J. C. 1996, ApJ, 470, 551

Draine, B. T., & Weingartner, J. C. 1997, ApJ, 480, 633

Westphal, A. J., Bechtel, H. A., Brenker, F. E., et al. 2014a, M&PS, 49, 1720
Westphal, A. J., Bechtel, H. A., Brenker, F. E., et al. 2014b, Sci, 345, 786
Zubko, V. G., Mennella, V., Colangeli, L., & Bussoletti, E. 1996, MNRAS, 282, 1321

van de Hulst, H. C. 1957, Light Scattering by Small Particles (New York:

Fabian, D., Henning, T., Jäger, C., et al. 2001, A&A, 378, 228

Kataoka, A., Muto, T., Momose, M., et al. 2015, ApJ, 809, 78

Martin, P. G. 1974, ApJ, 187, 461 Min, M., Hovenier, J. W., & de Koter, A. 2003, A&A, 404, 35

Ossenkopf, V., Henning, T., & Mathis, J. S. 1992, A&A, 261, 567 Press, W. H., Teukolsky, S. A., Vetterling, W. T., & Flannery, B. P. 1992,

Rho, J., Gomez, H. L., Boogert, A., et al. 2018, MNRAS, 479, 5101

Sargent, B., Forrest, W. J., D'Alessio, P., et al. 2006, ApJ, 645, 395

L. H. Aller (Chicago, IL: Univ. Chicago Press), 221 Hensley, B. S., & Draine, B. T. 2021, ApJ, 906, 73 Hensley, B. S., Zhang, C., & Bock, J. J. 2019, ApJ, 887, 159

Hoang, T., & Lazarian, A. 2008, MNRAS, 388, 117

Hoang, T., & Lazarian, A. 2009a, ApJ, 695, 1457 Hoang, T., & Lazarian, A. 2009b, ApJ, 697, 1316

Jones, R. V., & Spitzer, L. J. 1967, ApJ, 147, 943

Lazarian, A., & Hoang, T. 2007, MNRAS, 378, 910

Lazarian, A., & Roberge, W. G. 1997, ApJ, 484, 230

Lee, H. M., & Draine, B. T. 1985, ApJ, 290, 211

Martin, P. G. 1972, MNRAS, 159, 179

Cambridge: Cambridge Univ. Press)

Purcell, E. M., & Spitzer, L., Jr. 1971, ApJ, 167, 31

Rouleau, F., & Martin, P. G. 1991, ApJ, 377, 526

Silsbee, K., & Draine, B. T. 2016, ApJ, 818, 133

Treffers, R., & Cohen, M. 1974, ApJ, 188, 545

Tatsuuma, M., & Kataoka, A. 2021, arXiv:2101.04910

Weingartner, J. C., & Draine, B. T. 2003, ApJ, 589, 289

Tazaki, R., Lazarian, A., & Nomura, H. 2017, ApJ, 839, 56

Purcell, E. M. 1979, ApJ, 231, 404

**JQSRT**, 97, 161

489, 135

Continuous Media (Oxford: Pergamon) Lazarian, A., & Draine, B. T. 1999, ApJL, 520, L67

Greenberg, J. M. 1968, in Interstellar Grains, ed. B. M. Middlehurst &

Landau, L. D., Lifshitz, E. M., & Pitaevskii, L. P. 1993, Electrodynamics of

Min, M., Hovenier, J. W., Dominik, C., de Koter, A., & Yurkin, M. A. 2006,

Min, M., Hovenier, J. W., Waters, L. B. F. M., & de Koter, A. 2008, A&A,

Numerical recipes in FORTRAN. The Art of Scientific Computing (2nd ed.;

Gold, T. 1952, MNRAS, 112, 215

Hoang, T. 2019, ApJ, 876, 13